Journal of Marine Science and Application (2026) 25: 327-341
https://doi.org/10.1007/s11804-025-00615-6

RESEARCH ARTICLE

Numerical Investigation on Water Entry of Two-dimensional Wedges with a Moving Particle Semi-implicit Method

Chol Jun Pak[1], Min Hyok Jon[1], Yong Gwang Ri[1] and Ryong Il Ju[1]

Received: 27 November 2024 / Accepted: 26 January 2025

Abstract

The water entry problem is an important issue in the field of marine engineering, and predicting the behavior of a body entering water is extremely difficult because of water's strong nonlinearity. In this study, we investigate hydrodynamic load acting on a two-dimensional (2D) wedge during water entry. The adopted approach is the moving particle semi-implicit (MPS) method, which is widely utilized in the simulation of nonlinear free surface flow. Moreover, two techniques to enhance the performance of MPS are suggested and a symmetry domain technique for reducing the computational cost is also proposed. Additionally, a fluid–solid coupling algorithm using the MPS method is suggested. Several cases are numerically investigated to verify the proposed method, and its performance is verified through the simulation of hydrostatic pressure and dam break. Furthermore, 2D wedge water entry problems with symmetric or asymmetric characteristics are studied using the proposed MPS method and compared with some experimental and previous numerical studies. The results show that the MPS with the proposed schemes can provide a reliable numerical prediction for water entry problems.

Keywords Water entry; Moving particle semi-implicit method; Hydrodynamic load; Free falling; Fluid–solid coupling

1 Introduction

Predicting the hydrodynamic load on a body entering water is important to resolving problems in the field of marine engineering. When a ship moves in water, the hull experiences a high impact by the waves because of the relative motion between the ship and the waves. Thus, water entry adversely affects ship motion and can even damage the ship structure.

The original research on water entry was conducted by Von Karman (1929), who proposed a model based on the momentum theorem, which was a pioneer theory of water entry. Afterward, Wagner (1932) developed a model to predict impact pressure and studied two-dimensional (2D) water impact on a solid body. With regard to the water entry of wedges, Von Karman's method is very similar to that of Wagner's.

Water entry problems have been widely investigated with experimental, theoretical, and numerical methods.

Experiments play an important role in analyzing and resolving problems arising in engineering practice, and many experimental studies on the water entry of different objects, such as wedges and cylinders, have been conducted.

Most studies are related to the water entry of wedges. Zhao et al. (1996) conducted experimental studies on 2D water entry with and without flow separation. Xu et al. (1999) tested wedges freely dropped from different heights to predict the impact effect during water entry; in their experiment, they reported impact characteristics, such as instantaneous velocity and impact acceleration; given that the wedges were free to roll after water entry, the results showed an inertia effect in the roll direction. Judge et al. (2004) performed numerous experiments on the asymmetric water entry of wedges; their experimental results were in good agreement with those obtained using an analytical 2D vortex distribution method. Some experimental investigations on the water entry of wedge-shaped objects with constant velocities have been conducted (Yettou et al., 2006;

Article Highlights

- The hydrodynamic load on a body entering water must be predicted accurately to estimate its structural safety.
- Due to highly nonlinearity of free surface during water entry, the MPS method, one of particle methods utilized to simulate nonlinear free surface flows, is adopted to the water entry problem.
- Some techniques for improving the original MPS method are presented and compared with the analytic and experimental results.
- An algorithm for the fluid-solid coupling problem using the MPS method is presented and applied to the simulation of 2D wedge water entry.

✉ Chol Jun Pak
pcj83427@star-co.net.kp

[1] Faculty of Naval Architecture and Ocean Engineering, Kim Chaek University of Technology, Pyongyang 999093, Democratic People's Republic of Korea

Tveitnes et al., 2008; Wang et al., 2015). Barjasteh et al. (2016) investigated the asymmetric water entry of wedges, conducting several experiments with different dead-rise angles, inclination angles, and drop heights; the experimental results showed good agreement with different theories on water entry problem and indicated the considerable effect of inclination angle on impact pressure.

Sun and Faltinsen (2009) conducted an experimental investigation on the water entry of a bow flare ship section; their experiment focused on asymmetric entry and reported several characteristics, such as acceleration and impact pressure; the numerical and experimental results showed a very good agreement. Moreover, Wei and Hu (2014, 2015) experimentally investigated the water entry of a horizontal cylinder using a high-speed digital video camera; in their experiment, the hydrodynamic loads acted on the cylinder were reported, and high-quality images were provided for validation by other studies. Li et al. (2020) conducted experimental research on the water entry of various nosed projectiles with high velocities. She et al. (2021) investigated the water entry of a bulbous bow with a time-resolved particle image velocimetry system with good performance in capturing transient flow; they determined the pressure distribution around the bulbous bow during water entry and provided data for other studies.

Compared with experimental research, the theoretical and numerical investigations are time-saving and cost-saving.

Based on fully nonlinear potential flow theory, nonlinear numerical methods (Iafrati and Battistin, 2003; Xu et al., 2008; Riccardi and Iafrai, 2004; Bao et al., 2016; Bao et al., 2017) were developed to determine the free surface profile and hydrodynamic load on symmetric or asymmetric wedges during water entry. Sun et al. (2019) studied the water entry problem of a 2D wedge-shaped tank with liquid on the basis of velocity potential theory; in their work, two separated regions for the internal liquid and open water were created, and the fluid loads in these regions were estimated. Potential theory has also been applied to several water entry problems (Del Buono et al., 2021; Zekri et al., 2021), and Navier-Stokes equations have been used in studying water entry problems (Piro and Maki, 2013; Gu et al., 2014).

Complementary to these numerical studies, different CFD methods have been utilized in investigating water entry.

Wen and Qiu (2018) proposed a constrained interpolation profile to predict a three-dimensional (3D) water entry; in their work, density functions were adopted to improve an interface-capturing scheme, and an MPI-based parallel computing technology was used to accelerate computational speed. Sun and Faltinsen (2006), and Sun (2007) investigated a free surface profile during the water entry of a vertical cylinder; they used the boundary element method (BEM), and the results obtained agreed with experimental results. Wu (2012) suggested a high-order BEM for resolving water entry problems. Moreover, a semi-analytical hydrodynamic impact theory for analyzing the water entry of elastic wedges on the basis of modal superposition method, BEM and Wagner theory was developed (Yu et al., 2019; Zhang et al., 2021; Sun et al., 2021a).

Most CFD applications were implemented through smoothed particle hydrodynamics (SPH), mainly focusing on fluid–structure interaction (FSI) problems with respect to the fully nonlinear fluid flows (Oger et al., 2006; Farsi and Ghadimi, 2015; Luo et al., 2021; Khayyer et al., 2021; Gotoh et al., 2021; Chen et al., 2021). Sun et al. (2015) simulated free surface flow around a rigid body with a weakly compressible SPH method; they proposed a solid boundary technique to improve the stability of numerical solutions. Sun et al. (2018) also proposed a δ+-SPH model for 3D water entry problems and applied adaptive particle refinement to enhance computational efficiency. Meng et al. (2021) suggested a multiphase SPH model for water entry problems and a cutoff value of density for preventing negative pressure. Several GPU-accelerated SPH methods have been developed and used in investigating water entry problems. Zhang et al. (2022a) presented an accelerated SPH framework-based GPU for simulating 3D water entry problems, and Zhao et al. (2023) developed a multiphase and multiresolution SPH method using multi-GPU implementation for FSI problems, simulated the water entry of a projectile, and provided the resolution of up to 120 million particles by using multiple GPUs. All the numerical methods showed good performance in the simulation of different water entry problems.

Furthermore, the moving particle semi-implicit method has also been applied to simulate water entry problems. Zhang et al. (2022b) developed an MPS method with an adaptive variable-size particle model and verified their work by simulating dam break and water entry problems. Zha et al. (2021) suggested an improved higher-order MPS method for FSI problems and applied it to an elastic wedge water entry problem. Compared with the SPH method, the MPS method has not been widely applied to water entry problems.

The present study aims to investigate water entry problems of 2D wedges by using an MPS method and some handling techniques. This study is organized as follows: Section 2 addresses some schemes for improving the MPS method, a symmetric domain technique for reducing computational cost, and a fluid–solid-coupling algorithm using the MPS method. In Section 3, the proposed techniques are verified through several numerical investigations and discussed. Finally, some conclusions are described in Section IV.

2 Methodology

2.1 MPS method

2.1.1 Original MPS method

The continuity equation and Navier–Stokes equation for

incompressible viscous flows are governing equations in hydrodynamics and are expressed as follows:

$$\nabla \cdot \boldsymbol{u} = 0 \tag{1}$$

$$\frac{D\boldsymbol{u}}{Dt} = -\frac{1}{\rho}\nabla p + \nu\nabla^2\boldsymbol{u} + \boldsymbol{f} \tag{2}$$

where $\rho, \boldsymbol{u}, p, \nu$ denote the density, velocity, pressure, and kinematic viscosity of the fluid, respectively, and $\boldsymbol{f}$ is the body force.

The original MPS method was proposed by Koshizuka and Oka (1996); in their study, fluid particles are assumed to be interacting with each other, as indicated in the following weight function:

$$w\left(r, r_{\mathrm{e}}\right) = \begin{cases} \dfrac{r_{\mathrm{e}}}{r} - 1, & r < r_{\mathrm{e}} \\ 0, & r \geqslant r_{\mathrm{e}} \end{cases} \tag{3}$$

where r denotes the distance between two particles and r_{e} is the radius of the influential domain. On the basis of this weight function, the fluid density and differential operators are defined.

The particle number density, i.e., the fluid density, is defined as

$$n_i = w\left(\left|\boldsymbol{r}_j - \boldsymbol{r}_i\right|, r_{\mathrm{e}}\right) \tag{4}$$

where $\boldsymbol{r}_i$, $\boldsymbol{r}_j$ are the positions of particles i and j, respectively.

The gradient and Laplacian operator are formulated as

$$\nabla\phi_i = \frac{d}{n^0}\sum_{j\neq i}\left[\frac{\phi_j - \phi_i}{\left|\boldsymbol{r}_j - \boldsymbol{r}_i\right|^2}\left(\boldsymbol{r}_j - \boldsymbol{r}_i\right)w\left(\left|\boldsymbol{r}_j - \boldsymbol{r}_i\right|, r_{\mathrm{e}}\right)\right] \tag{5}$$

$$\nabla^2\phi_i = \frac{2d}{n^0\lambda^0}\left(\phi_j - \phi_i\right)w\left(\left|\boldsymbol{r}_j - \boldsymbol{r}_i\right|, r_{\mathrm{e}}\right) \tag{6}$$

$$\lambda^0 = \frac{\sum_{j\neq i}\left|\boldsymbol{r}_j - \boldsymbol{r}_i\right|^2 w\left(\left|\boldsymbol{r}_j - \boldsymbol{r}_i\right|, r_{\mathrm{e}}\right)}{\sum_{j\neq i} w\left(\left|\boldsymbol{r}_j - \boldsymbol{r}_i\right|, r_{\mathrm{e}}\right)} \tag{7}$$

where ϕ is an arbitrary scalar quantity, d is the number of space dimensions, n^0 is the particle number density at the initial arrangement, and λ^0 is the correction parameter of the Laplacian operator.

The computational procedure of the MPS method mainly consists of two stages. First, fluid particles' velocities and positions at the intermediate time step are determined. The intermediate quantities $\boldsymbol{u}_i^*$ and $\boldsymbol{r}_i^*$ are calculated by velocity $\boldsymbol{u}_i^k$ and position $\boldsymbol{r}_i^k$ at the current time step k as follows:

$$\boldsymbol{u}_i^* = \boldsymbol{u}_i^k + \Delta t\boldsymbol{g} + \nu\nabla^2\boldsymbol{u}_i^k\Delta t \tag{8}$$

$$\boldsymbol{r}_i^* = \boldsymbol{r}_i^k + \Delta t\boldsymbol{u}_i^* \tag{9}$$

where Δt and $\boldsymbol{g}$ denote time interval and acceleration of gravity, respectively.

Then, the fluid particles' velocities and positions at the next time step are updated. In this stage, the fluid particles' pressure is calculated by solving the pressure Poisson equation (PPE).

$$\nabla^2 p = -\frac{\rho}{\Delta t^2}\frac{n^* - n^0}{n^0} \tag{10}$$

where n_i^* is the particle number density at the intermediate time step. The PPE can be solved by different iterative solvers, such as the conjugate gradient (Hestenes and Stiefel, 1952) and generalized minimal residual methods (Saad and Schultz, 1986; Amritkar et al., 2015). After the fluid particles' pressure is calculated, their velocities and positions at the next time step $k+1$ are updated as follows:

$$\boldsymbol{u}_i^{k+1} = \boldsymbol{u}_i^* - \frac{\Delta t}{\rho}\nabla p_i^{k+1} \tag{11}$$

$$\boldsymbol{r}_i^{k+1} = \boldsymbol{r}_i^k + \Delta t\boldsymbol{u}_i^{k+1} \tag{12}$$

Given that the original MPS method has many drawbacks, we adopted some modifications to the original MPS method. Checking free surface particles correctly is crucial to ensuring the stability of a solution. To date, substantial effort has been devoted to improving free surface identification (Marrone et al., 2010; Shibata et al., 2015a; Shibata et al., 2015b). Our numerical studies have shown that the identification method proposed by Shibata et al. (2015b) is effective. Thus, we used it to identify free surface particles.

Furthermore, owing to unphysical pressure fluctuation arising from the original PPE source term, many modifications to PPE have been proposed. In this study, we used the PPEs proposed by Sun et al. (2021b) to obtain smooth pressure distribution.

$$\nabla^2 p_i = \frac{\rho}{\Delta t}\nabla \cdot \boldsymbol{u}_i^* + \gamma\frac{\rho}{\Delta t^2}\frac{n^0 - n_i}{n^0} \tag{13}$$

where γ is a relaxation coefficient, which is 0.01 in this study.

In addition, the gradient model from Khayyer and Gotoh (2008) was used in this study.

$$\nabla p_i = \frac{d}{n^0}\sum_{j\neq i}\left[\frac{p_j + p_i}{\left|\boldsymbol{r}_j - \boldsymbol{r}_i\right|^2}\left(\boldsymbol{r}_j - \boldsymbol{r}_i\right)w\left(\left|\boldsymbol{r}_j - \boldsymbol{r}_i\right|, r_{\mathrm{e}}\right)\right] \tag{14}$$

This gradient model ensures the conservation of momentum and correctly represents the action–reaction physical law.

2.1.2 Some techniques for improving the original MPS method

2.1.2.1 Laplacian compensation in the region close to the wall boundary

One of the shortcomings of the original MPS method is the lack of neighboring particles of fluid particles in the region close to the wall boundary. This problem leads to the incorrect calculation of the Laplacian operator of the fluid particles' pressure and thus decreases the accuracy of the calculated pressure. One way to resolve this problem is to add fluid particles in the region. This approach guarantees the accuracy of pressure calculated by Laplacian compensation.

In the present study, we considered one layer of wall particles and several layers of virtual particles beyond the wall boundary (Figure 1). Virtual particles are generated by the corresponding wall particle, that is,

$$\boldsymbol{r}_v = \boldsymbol{r}_w + s\boldsymbol{n}\,;\ s = Kl_0, K = 1, 2, \cdots \tag{15}$$

where $\boldsymbol{r}_w$ is the position of a wall particle, $\boldsymbol{r}_v$ is the position of virtual particles generated by this wall particle, l_0 is the initial spacing, $\boldsymbol{n}$ is the normal unit vector to the wall boundary, and s is the distance between the virtual particle and corresponding wall particle.

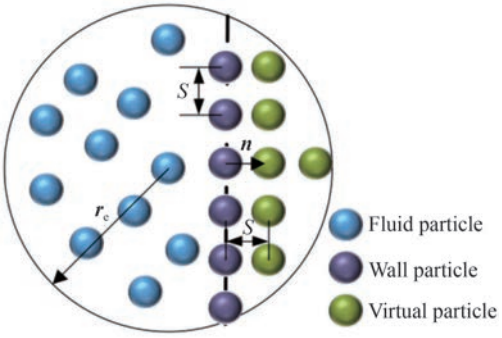

Figure 1 Generation of virtual particles

After several modifications are implemented, the pressure of the virtual particle can be expressed as follows:

$$P_v = P_w + \rho s\boldsymbol{n} \cdot \left(-\dot{\boldsymbol{U}} + \nu\nabla^2\boldsymbol{U} + \boldsymbol{g}\right) \tag{16}$$

where P_v and P_w denote the pressure of virtual and wall particles, respectively; ρ is the fluid density; $\boldsymbol{U}$ and $\dot{\boldsymbol{U}}$ are the velocity and acceleration of the wall particles, respectively.

The Laplacian operator of pressure at a fluid particle i close to the wall boundary can be calculated as follows:

$$\left\langle \nabla^2 P \right\rangle_i = \frac{2d}{n^0\lambda^0}\left(\sum_{j\in\Lambda_i^r}\left(P_j - P_i\right)w\left(\left|\boldsymbol{r}_j - \boldsymbol{r}_i\right|, r_e\right) + \sum_{j\in\Lambda_i^d}\left(P_{j'} - P_i\right)w\left(\left|\boldsymbol{r}_{j'} - \boldsymbol{r}_i\right|, r_e\right)\right) \tag{17}$$

where Λ_i^r denotes a set of real particles in the support domain of particle i and Λ_i^d denotes a set of virtual particles inside the support domain of particle i. In this equation, the second term within parentheses is the Laplacian compensation of pressure at particle i. Thus, the accuracy of the calculated pressure of fluid particles will be further improved relative to that obtained with the original MPS method.

2.1.2.2 Collision model between fluid and wall particles

Fluid particles tend to penetrate the wall boundary in the original MPS method. This phenomenon is more frequent for fluid particles with high velocities.

To address this problem, a collision model between fluid and wall particles has been suggested. The diagram of the collision model is shown in Figure 2.

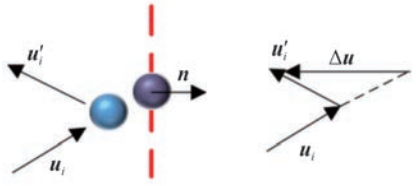

Figure 2 Diagram of the collision model between a fluid particle and a wall particle

If the distance between fluid particle i and wall particle j is smaller than a certain threshold value, fluid particle i collides with wall particle j (Figure 2). The velocity of fluid particle i is corrected as follows:

$$\boldsymbol{u}_i' = b\left(\boldsymbol{u}_i + \Delta\boldsymbol{u}\right) \tag{18a}$$

$$\Delta\boldsymbol{u} = \begin{cases} -2\left(\boldsymbol{u}_i \cdot \boldsymbol{n}\right)\boldsymbol{n}, & \left|\boldsymbol{r}_i - \boldsymbol{r}_j\right| < al_0 \\ 0, & \left|\boldsymbol{r}_i - \boldsymbol{r}_j\right| \geqslant al_0 \end{cases} \tag{18b}$$

where $\Delta\boldsymbol{u}$ denotes the correction value; $\boldsymbol{n}$ is the normal unit vector to the wall boundary; $\boldsymbol{u}_i$ and $\boldsymbol{u}_i'$ are the velocities of a fluid particle before and after the collision, respectively; a and b are the adjusting parameters, which were empirically set at 0.6–0.7 and 0.2–0.5, respectively, in this study.

In addition, we assumed that the collision was an elastic collision and the wall was stationary. In ocean engineering practice, most problems are related to the moving boundary. The collision model can be easily modified for the moving boundary as follows:

$$\boldsymbol{u}_i' = b\left(\boldsymbol{u}_i'' + \Delta\boldsymbol{u}\right) \tag{19a}$$

$$\boldsymbol{u}_i'' = \boldsymbol{u}_i - \boldsymbol{u}_j \tag{19b}$$

$$\Delta\boldsymbol{u} = \begin{cases} -2\left(\boldsymbol{u}_i'' \cdot \boldsymbol{n}\right)\boldsymbol{n}, & \left|\boldsymbol{r}_i - \boldsymbol{r}_j\right| < al_0 \\ 0, & \left|\boldsymbol{r}_i - \boldsymbol{r}_j\right| \geqslant al_0 \end{cases} \tag{19c}$$

where $\boldsymbol{u}_i$ and $\boldsymbol{u}_j$ denote the velocity of fluid and wall particles before the collision, respectively; $\boldsymbol{u}_i''$ is the relative velocity of a fluid particle to a wall particle.

2.1.3 Symmetric domain technique

If a simulation domain flow has a symmetrical characteristic, the cost of the computation can be reduced by considering the "half-domain" rather than the "whole-domain". In other words, only the half of the simulation domain is simulated. In the present study, a handling technique for the symmetric domain is suggested, and a model for symmetric water entry is considered.

Figure 3 shows the schematic of the symmetric domain simulation. The initial arrangement of fluid particles is shown in Figure 3(a). Let a domain of distance $4l_0$ away from the Y axis toward the $-x$ direction denote the "image domain", and all the fluid particles inside the image domain denote "image particles" (Figure 3(b)). The image particles are generated by symmetrizing fluid particles within the domain of distance $4l_0$ away from the Y axis toward the $+x$ direction. The flow in the region close to the Y axis can be modeled correctly by integrating the physical quantities of image particles into the following equation:

$$\left\langle r_x \right\rangle_{i'} = -\left\langle r_x \right\rangle_i, \left\langle r_y \right\rangle_{i'} = \left\langle r_y \right\rangle_i \tag{20a}$$

$$\begin{cases} \left\langle v_x \right\rangle_{i'} = -\left\langle v_x \right\rangle_i \\ \left\langle v_y \right\rangle_{i'} = \left\langle v_y \right\rangle_i \\ P_{i'} = P_i \end{cases} \tag{20b}$$

where the subscripts i' and i denote the image and fluid particle, respectively; r_x, r_y denote the coordinates of particles in the x, y directions, respectively; P denotes the pressure of particles; v_x, v_y denote the velocity components in the x, y directions, respectively.

These image particles are considered in the calculation of fluid particles close to the symmetric plane. This principle is the same as adding virtual particles in Laplacian compensation. This technique not only reduces computational time but also reduces consumed memory by half, compared with whole-domain simulation. Notably, image particles are dynamically generated in every time step, and handling is only implemented in symmetric flow simulation.

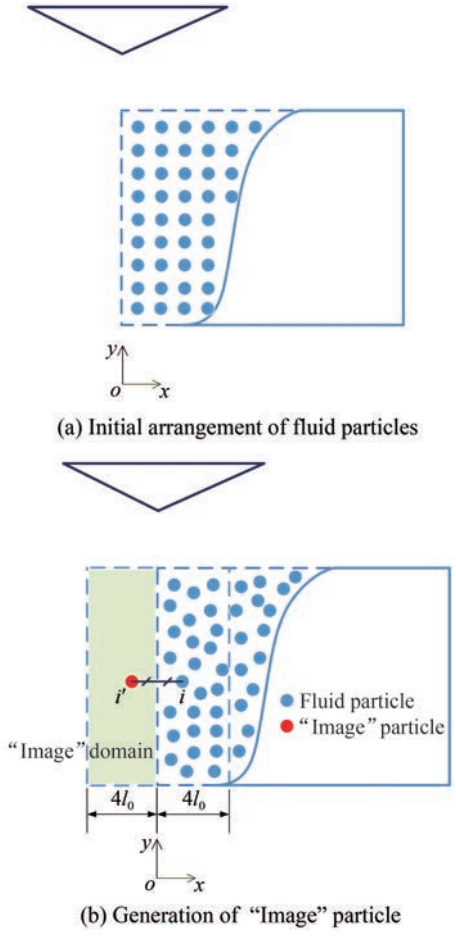

Figure 3 Schematic of symmetric domain simulation

2.2 Fluid–solid-coupling algorithm

2.2.1 Governing equations for fluid–solid-coupling problem

The motion of a solid can be considered the resultant motion of translation and rotation. Therefore, the velocity of any position in a solid can be evaluated by the translational velocity of its centroid and rotational velocity around its centroid. Based on the conservation principle of momentum and moment momentum, the translational and rotational acceleration of a solid's centroid are determined by the following equations (Sun et al., 2018):

$$M \frac{\mathrm{d}\boldsymbol{U}_c}{\mathrm{d}t} = \boldsymbol{F}_{f-s} + M\boldsymbol{g} \tag{21}$$

$$I \frac{\mathrm{d}\boldsymbol{\Omega}_c}{\mathrm{d}t} = \boldsymbol{T}_{f-s} \tag{22}$$

where the subscript c denotes the centroid of a solid, $\boldsymbol{U}_c$ is the translational velocity of the centroid, $\boldsymbol{\Omega}_c$ is the rotational velocity around the centroid, M is the mass of the solid, I is the moment of inertia, and $\boldsymbol{F}_{f-s}$ $\boldsymbol{T}_{f-s}$ are the resultant force and moment acted on the solid from the fluid, respectively.

After the translational velocity $\boldsymbol{U}_c$ and rotational velocity $\boldsymbol{\Omega}_c$ are determined with Equations (21) and (22), the velocity at any position over a solid boundary is calculated as follows:

$$\boldsymbol{v}_b = \boldsymbol{U}_c + \boldsymbol{\Omega}_c \times \left(\boldsymbol{r}_b - \boldsymbol{r}_c\right) \tag{23}$$

where $\boldsymbol{r}_b$ and $\boldsymbol{r}_c$ are the positions of any point over the boundary and a solid's centroid, respectively.

2.2.2 Fluid–solid interaction

Solving Equations (21) and (22) is crucial for the fluid–solid coupling simulation. The resultant force and moment acted on a solid from a fluid can be calculated if the pressure on the solid boundary is known.

In the present study, the fluid–solid interaction is implemented according to the following process. In every time step, the MPS simulation is first performed, and the pressure of wall particles is determined. Then, the $\boldsymbol{F}_{f-s}$ and $\boldsymbol{T}_{f-s}$ values of all the wall particles are calculated by the following formula:

$$\boldsymbol{F}_{f-s} = \sum_i P_i \Delta S_i \boldsymbol{n}_i \tag{24}$$

$$\boldsymbol{T}_{f-s} = \sum_i \left(\boldsymbol{r}_i - \boldsymbol{r}_c\right) \times \left(P_i \Delta S_i \boldsymbol{n}_i\right) \tag{25}$$

where the subscript i denotes the index of the wall particles, P_i is the pressure of wall particles, ΔS_i is the boundary surface's infinitesimal area, $\boldsymbol{n}_i$ is the normal vector to the boundary, and $\boldsymbol{r}_i$ is the position vector of the wall particles. We can argue that $\Delta S_i = l_0^2$. The translational velocity $\boldsymbol{U}_c$ and rotational velocity $\boldsymbol{\Omega}_c$ of the centroid of the solid are updated by Equations (21) and (22), respectively. Finally, the velocities of wall particles $\boldsymbol{v}_b$ are calculated using Equation (23), and the positions of the wall particles are updated as follows:

$$\boldsymbol{r}_b^{new} = \boldsymbol{r}_b + \boldsymbol{v}_b \Delta t \tag{26}$$

where $\boldsymbol{r}_b^{new}$ denotes the updated position of wall particles, and Δt is the time step.

The algorithm for fluid-solid coupling is illustrated in Figure 4.

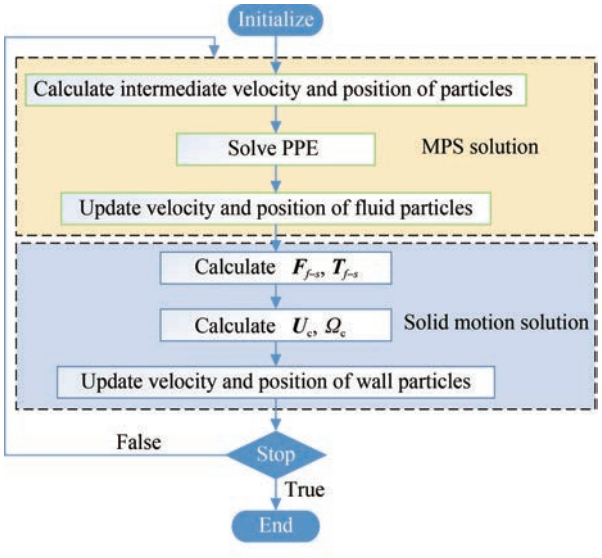

Figure 4 Algorithm for fluid–solid coupling problem

3 Numerical results and discussions

The main goal of the present study is to investigate the water entry problem by using the MPS method. To validate our suggestions, we numerically studied hydrostatic pressure and dam break problems and verified the proposed MPS method. Then, the water entry problems of 2D wedges were investigated using the MPS method, and the results were compared with experimental and previous numerical results.

3.1 Validation of the present MPS method

3.1.1 Hydrostatic pressure problem

The hydrostatic pressure problem is one of the problems widely used in validating the performance of particle methods. Figure 5 shows the geometry for the hydrostatic pressure problem. The tank is filled with fresh water to 0.4 m. Pressure is captured at a measuring point P and compared with an analytical solution. The simulations are conducted with different particle spacings, i. e. l_0 = 0.006, 0.008, 0.01, 0.012 m. The time step is 1.0×10^{-3} s, and the physical simulation time is 5 s.

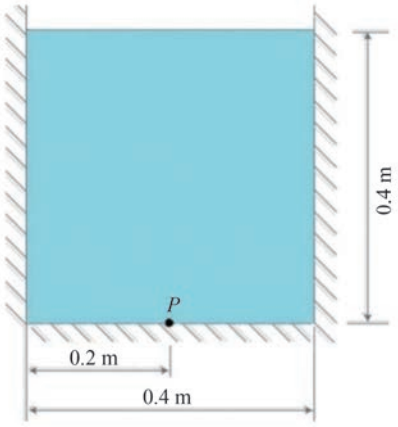

Figure 5 Geometric model for hydrostatic pressure problem

Figure 6 shows the comparison between analytic pressure and MPS pressure at measuring point P. In this figure, MPS results correspond to 0.006 m particle spacing. Figure 6(a) depicts the comparison of the analytic pressure and the result of MPS without Laplacian compensation, whereas Figure 6(b) shows the comparison of the analytic pressure and the result of MPS with Laplacian compensation. As can be seen in Figure 6, Laplacian compensation greatly enhances the accuracy of the MPS method, and pressure fluctuation is suppressed when the method is applied.

Table 1 shows the averaged relative errors of pressure at measuring point P at different particle spacings. These errors are calculated as the relative deviation of the MPS results from the analytical pressure and time averaged by averaging from 2 s to 5 s. When l_0 = 0.006 m, the relative

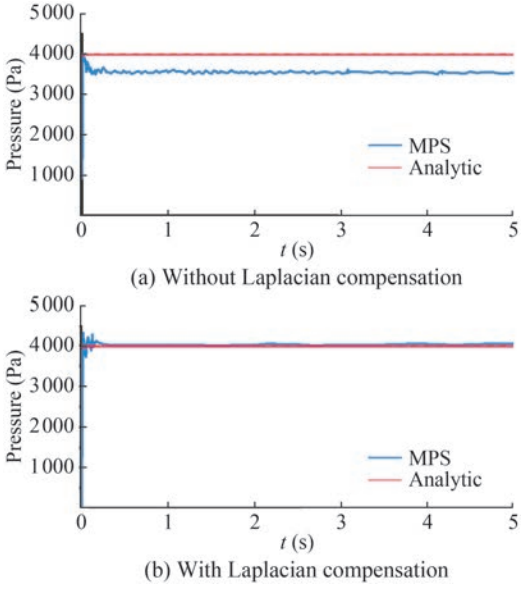

Figure 6 Comparison between analytic pressure and MPS pressure at measuring point *P*

Table 1 Relative errors according to different particle distances (%)

Laplacian compensation	l_0 (m)			
	0.006 m	0.008 m	0.010 m	0.012 m
No	−8.78	−9.32	−9.49	−9.79
Yes	0.22	0.27	0.71	0.75

errors are 0.22 and −8.78 with and without Laplacian compensation, respectively. This result implies the effectiveness of Laplacian compensation and obtained in other particle spacings. Laplacian compensation exerts a good effect on the performance of the MPS method (Table 1), and relative error decreases with particle spacing. Therefore, a small particle spacing provides high accuracy.

Figure 7 shows the particles' arrangement and pressure distribution obtained when $t = 5$ s and $l_0 = 0.006$ m. The particles are evenly distributed, and the pressure distribution has smooth and reasonable characteristics.

The above results demonstrate that Laplacian compensation considerably improves the performance of the MPS method.

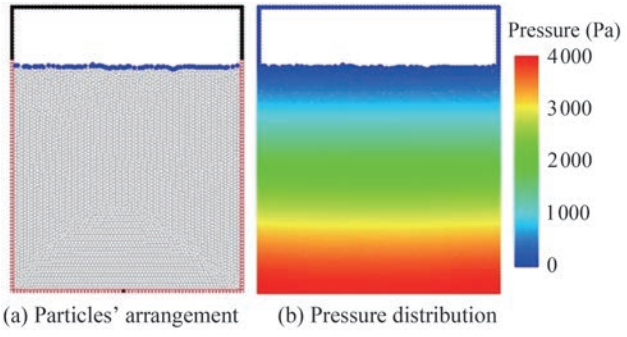

Figure 7 Particles' arrangement and pressure distribution at $t = 5$ s

3.1.2 Dam break problem

The dam break problem is a typical problem for verifying the particle method. For the validation of the present MPS method, the dam break problem is simulated and compared with the experimental data of Lobovsky et al. (2014). The geometry model for the dam break simulation is illustrated in Figure 8. Four measuring points are at the same positions in the experiment (Lobovsky et al., 2014): 0.003, 0.015, 0.03, and 0.080 m along the vertical direction. The particle spacing is 0.005 m, and the number of total particles is 14964. The time step is set at 5×10^{-4} s.

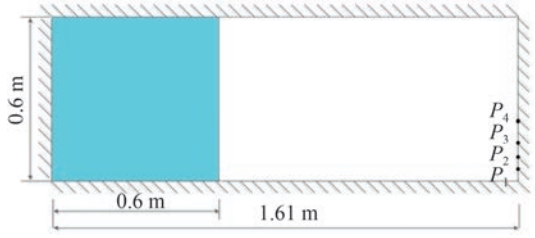

Figure 8 Geometry model for the dam break problem

Figure 9 shows the time histories of pressure at four measuring points obtained with the experiment and MPS method, here *H* is a height of water in Figure 8, i.e., 0.6 m. As shown in Figure 9, the results of MPS with Laplacian compensation are in good agreement with the experimental data. However, the results of MPS without Laplacian compensation show severe fluctuation, demonstrating that Laplacian compensation enhances the performance of the MPS method.

To validate the collision model between fluid and wall particles, we used the MPS results obtained at $t = 0.397$ s (Figure 10). When the MPS method was performed without the collision model, two particles penetrated the wall boundary, as shown in Figure 10(a). Conversely, when the collision model was adopted, no fluid particle penetrated the wall boundary. These findings demonstrate that the proposed collision model works efficiently.

Figure 11 depicts the pressure distribution obtained at different times from the present MPS method. The pressure distributions are smooth and reasonable physically, and the proposed MPS method shows good performance in the simulation of the dam break problem.

3.2 Investigation into the 2D wedge water entry problem with the present MPS method

In this subsection, the symmetric and asymmetric water entry of a 2D wedge were investigated using the MPS method and compared with some benchmark experiments and other numerical simulations. In the symmetric water entry problem, the symmetric domain technique was validated.

3.2.1 Symmetric water entry

The experimental model by Zhao et al. (1996) is widely

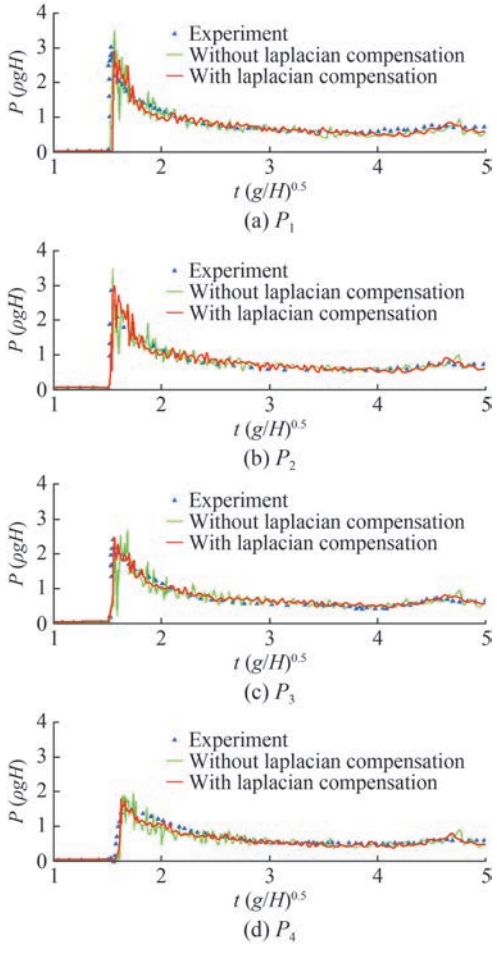

Figure 9 Time histories of pressure at different measuring points from the experiment and MPS without or with Laplacian compensation

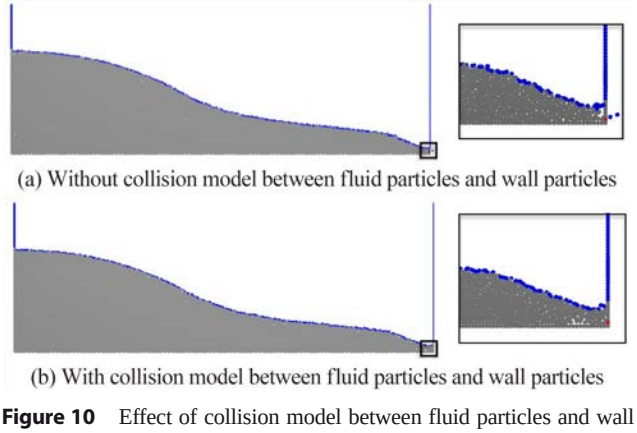

Figure 10 Effect of collision model between fluid particles and wall particles (t = 0.397 s)

used in investigating water entry problems. It was selected as a criterion in our study. Figure 12 depicts the geometry for the simulation of 2D wedge water entry. The dimensions of the wedge are the same as in the experimental model. The width (b) and dead-rise angle (β) of the wedge are 0.5 m and 30°, respectively, and the mass (M) of the wedge is 72.5 kg. In this simulation, the depth (D) and width (B)

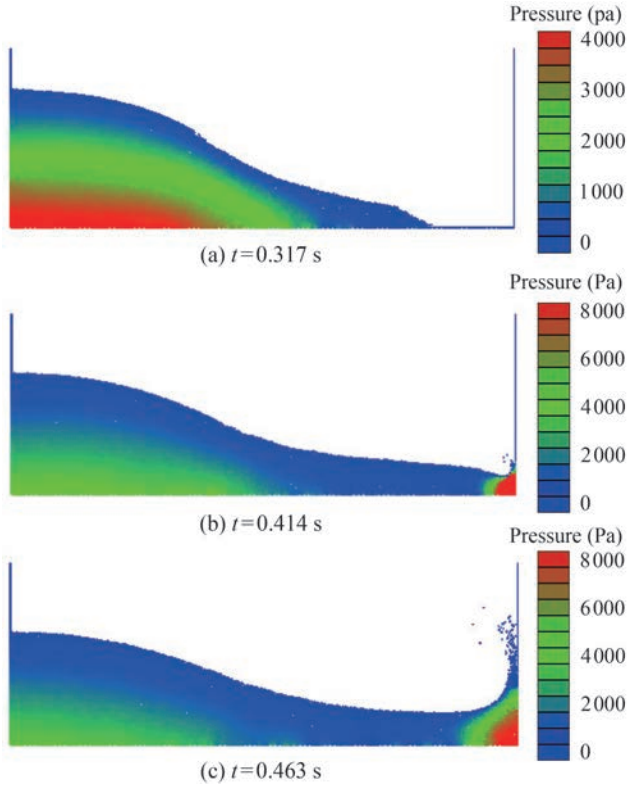

Figure 11 Pressure distribution obtained at different times from the present MPS

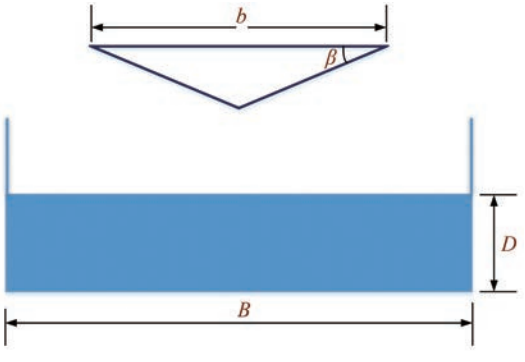

Figure 12 Geometry for the simulation of 2D wedge water entry

of the simulation domain are 1.0 and 2.0 m, respectively, l_0 = 0.01, 0.008, 0.005 m, and the total number of particles are 20759, 32201, and 81517, respectively.

Figure 13 shows the time history of the vertical velocity of a wedge during water entry. The MPS result was compared with the experiment (Zhao et al., 1996) and SPH results (Zhao et al., 2023). As shown in Figure 13, the MPS result agrees well with the experimental and SPH results. Figure 14 illustrates the time history of the vertical force acting on the wedge during water entry. In Figure 14, the vertical force by the MPS simulation is in good agreement with the experiment and below 17.5 ms when l_0 = 0.005 m. However, the MPS result is inferior to the experiment and SPH results in the other particle spacings, possibly because the high-order Laplacian model was not adopted.

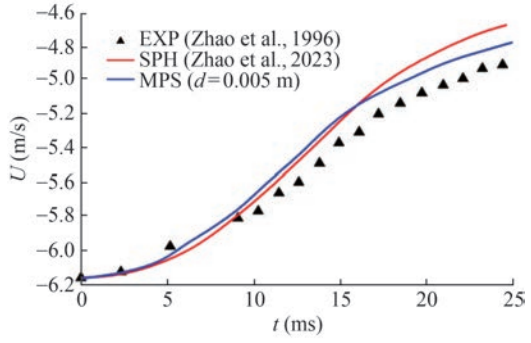

Figure 13 Time history of the vertical velocity during water entry

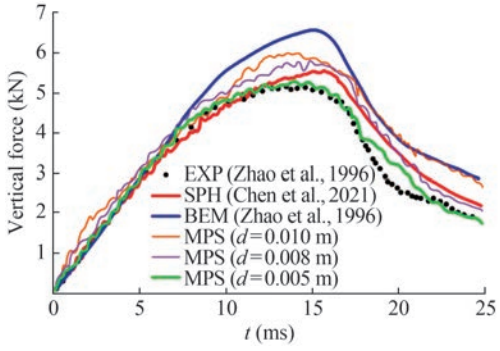

Figure 14 Time history of the vertical force acting on the wedge during water entry

For the validation of the results, especially those obtained with the symmetric domain technique, the 2D wedge water entry problem, which was the same as that in another experiment (Yettou et al., 2006), was investigated with the present MPS method. The dimensions of the wedge are the same as those of the wedge used in the experiment (Yettou et al., 2006). Figure 15 shows the geometry of a wedge with two pressure sensors at its edges. The width of the wedge is 1.2 m. We selected one test configuration from the several test configurations of the experiment. The characteristics of the test configuration are as follows: deadrise angle of the wedge 25°; wedge mass, 94 kg; and drop height, 1.3 m. The width and depth of the simulation domain are 2.0 and 1.0 m, respectively. The MPS simulations were conducted when l_0 = 0.006, 0.008, and 0.010 m.

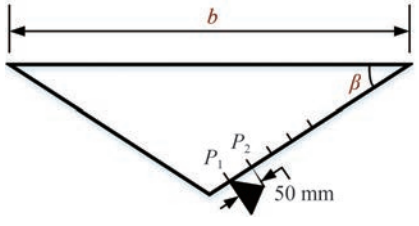

Figure 15 Geometry of the wedge

Figure 16 shows the time history of the wedge velocity during water entry from the drop height. In Figure 16, the result of MPS agrees well with that of experiment conducted by Yettou et al., (2006) and SPH (Zhang et al., 2022a) until time reaches approximately 0.55 s. Beyond this time, the MPS result deviates from the experiment and SPH simulation results, but the total trend is similar to that in the experiment.

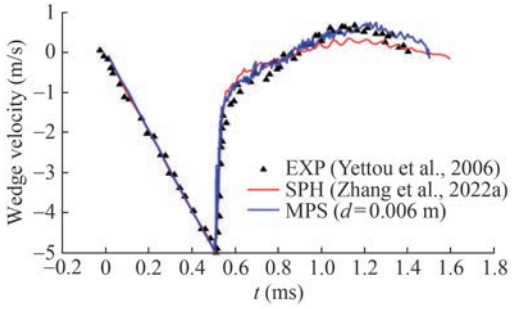

Figure 16 Time history of the wedge velocity during water entry

Figure 17 depicts the time history of the wedge velocity predicted by experiments (Zhao et al., 1996; Yettou et al., 2006), Von Karman (1929), Wagner (1932), and the present MPS method. The MPS result is extremely close to that of Wagner's results but does not agree well with the experimental results (Zhao et al., 1996; Yettou et al., 2006). The possible reason is the large particle spacing. However, the trend of the MPS result is similar to that of the experiment results (Figure 18). Figure 18 shows the comparison of the pressure obtained at P_1 and P_2 sensors during the experiment (Yettou et al., 2006), SPH simulation (Zhang et al., 2022a), and the present MPS simulation. Figure 18 shows the suppressed fluctuation in pressure and a trend close to the SPH results at a small particle spacing. However, the numerical results differ from the experimental results.

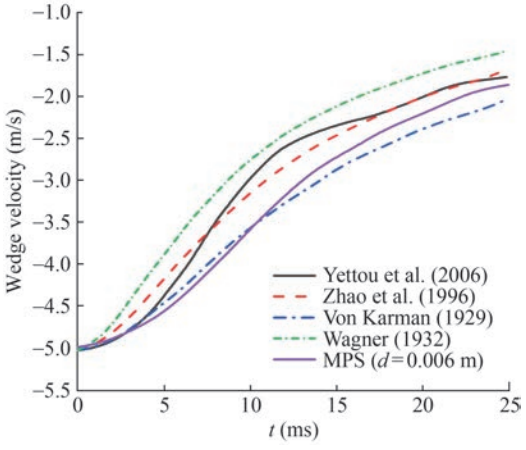

Figure 17 Time history of the wedge velocity during a certain period of impact after water entry

Figure 19 shows the pressure distributions obtained at different times during water entry when l_0 = 0.006 m. In Figure 19, the pictures on the left show the results from the whole-domain simulation, and the pictures on the right

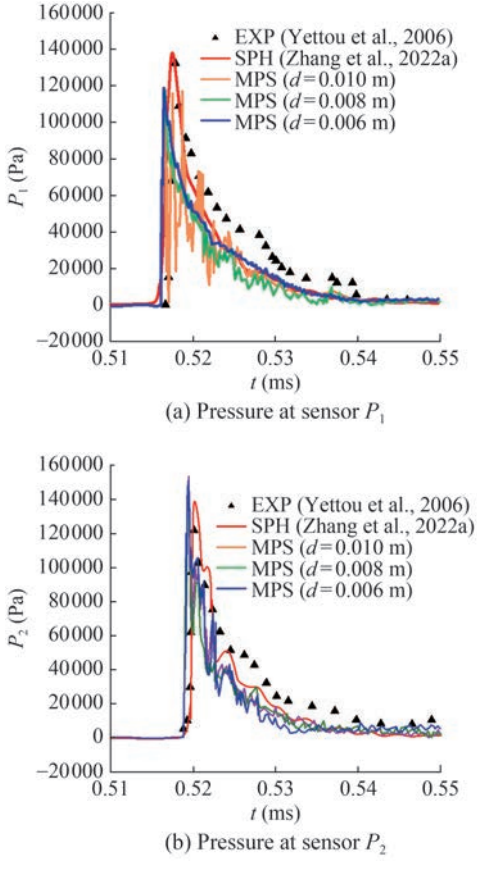

Figure 18 Time histories of the pressure at P_1 and P_2 sensors

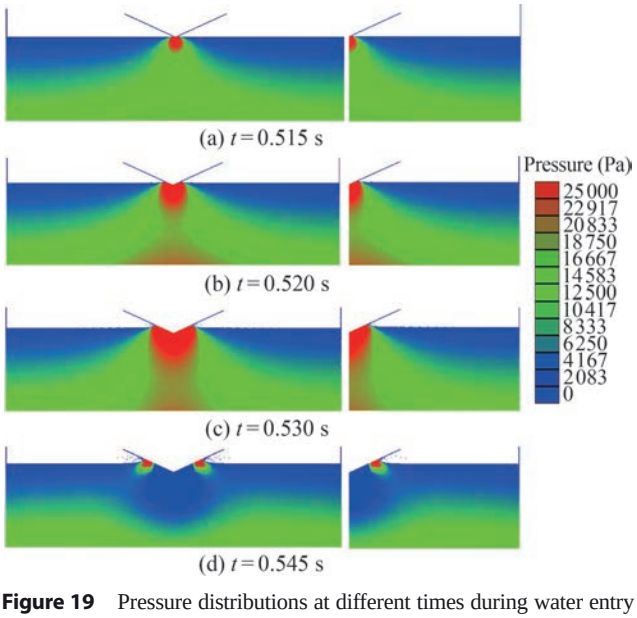

Figure 19 Pressure distributions at different times during water entry (Left: whole-domain simulation; Right: half-domain simulation)

show the results from the symmetric domain simulation. In these simulations, the total numbers of particles are 113 946 and 57 214, respectively, and the average computational times per time step are approximately 38 and 10 s, respectively. As can be seen in Figure 19, the pressure distributions from the two simulations are extremely similar. This finding shows that the symmetric domain technique not only considerably reduces the computational cost but also has an accuracy comparable to that of the whole-domain simulation. Thus, in the following simulations, the symmetric domain technique was adopted for the flow with symmetric characteristics.

3.2.2 Asymmetric water entry

The asymmetric water entry of a 2D wedge was investigated with the present MPS method. For comparison, the experiment (Barjasteh et al., 2016) was selected as a criterion, and the simulation was conducted on the same model used in the experiment (Barjasteh et al., 2016). Figure 20 depicts the wedge geometry for asymmetric entry. As to the asymmetric entry, the inclination angle (φ) is not zero. The mass (M) of the wedge is 44 kg, and l_0 = 0.004, 0.006, 0.008 m. The configurations of the simulation are listed in Table 2, where β and φ denote the dead-rise and inclination angles of the wedge, respectively.

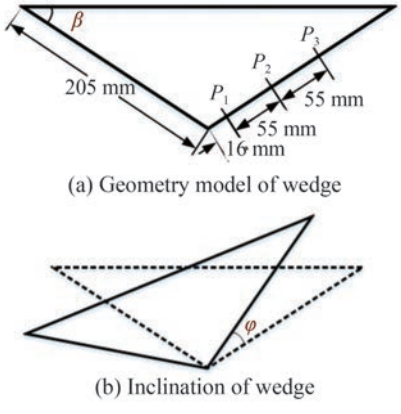

Figure 20 Wedge geometry for asymmetric entry

Table 2 Configurations of the simulation

No	Type of entry	β	φ	Drop height (m)
1	Symmetric	15	0	0.2, 0.5, 0.75
2		20	0	0.2, 0.5, 0.75
3		25	0	0.2, 0.5, 0.75
4		30	0	0.2, 0.5, 0.75
5	Asymmetric	20	5	0.5
6		20	10	0.5
7		20	15	0.5
8		30	10	0.5

First, symmetric water entry was investigated for a comparison with the experimental result. Figure 21 shows the time histories of pressure obtained at different sensors in different cases. The numerical results are in good agreement with the experiment at a small particle spacing. Peak pressure varies according to drop height: approximately

30, 47, and 230 kPa at 0.2, 0.5, and 0.75 m, respectively. The times when the peak pressure is observed also vary: approximately 12 ms at a drop height of 0.2 m and below 5 ms at a drop height of 0.5 and 0.75 m. The wedge dropped at a higher height produces a larger peak pressure, and the peak pressure appears at a later time when the wedge was dropped at a lower height.

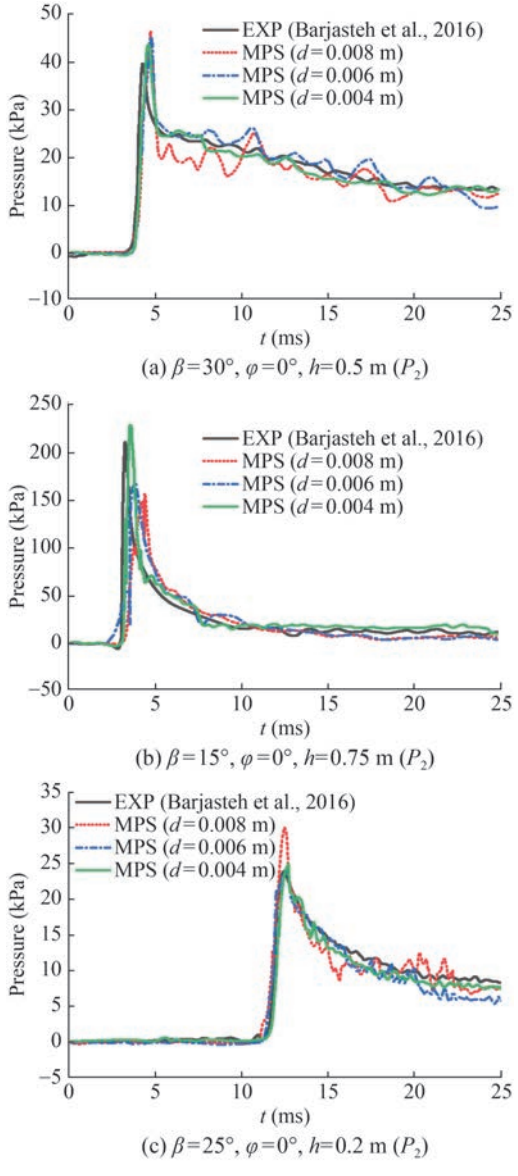

Figure 21 Time histories of pressure at different sensors in different cases

Figure 22 shows the pressure distributions obtained at different times with different dead-rise angles. In this figure, the left side corresponds to β = 20°; and the right side, β = 30°. As shown in Figure 22, the wedge with a small dead-rise angle is subjected to a large impact pressure. This finding is physically reasonable.

Asymmetric water entry was investigated. Figure 23

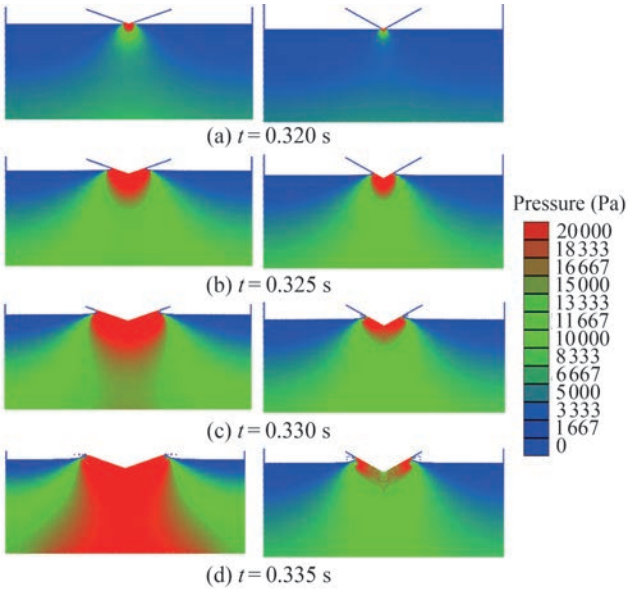

Figure 22 Pressure distribution at different times when h = 0.5 m (left: β = 20°, right: β = 30°)

shows the time histories of pressure at the P_1, P_2, and P_3 sensors during asymmetric entry. MPS simulation was conducted at a particle spacing of 0.004 m. Pressure measurements at P_1, P_2, and P_3 were plotted from left to right in every figure. Regarding the dead-rise angle, i. e., (a) and (b) or (c) and (d) in Figure 23, not only peak pressure but also the speed of impact occurrence increases with the inclination angle. At the same inclination angle, not only the peak pressure but also the speed of impact occurrence increases with decreasing dead-rise angle. The numerical results somewhat vary among the experimental results particularly when β = 30° but are in good agreement with the experiment results in terms of trend.

Figure 24 illustrates the compared results of the symmetric and asymmetric entry of the wedge. The numerical results somewhat vary from the experimental ones, but they have similar trends. When β = 20°, φ = 5° or φ = 0°, the difference between the numerical and experimental results is comparatively large, and the occurrence time of peak pressure slightly differs between symmetric and asymmetric entry. However, when β = 30°, φ = 10° or φ = 0°, the difference is small, and the occurrence time of peak pressure differs between symmetric and asymmetric entry, i.e., peak pressure appears earlier during asymmetric entry. Figure 24 shows that the hydrodynamic characteristics of the wedge during symmetric and asymmetric entry are similar at small dead-rise and inclination angles.

Figures 25 and 26 show the pressure distributions obtained at different times during the symmetric and asymmetric entry of the wedge at different dead-rise angles. In Figure 25, the pressure distributions have smooth characteristics, except when t = 0.330, 0.336 s. This feature can also be observed in Figure 26. Both figures show nonsmooth

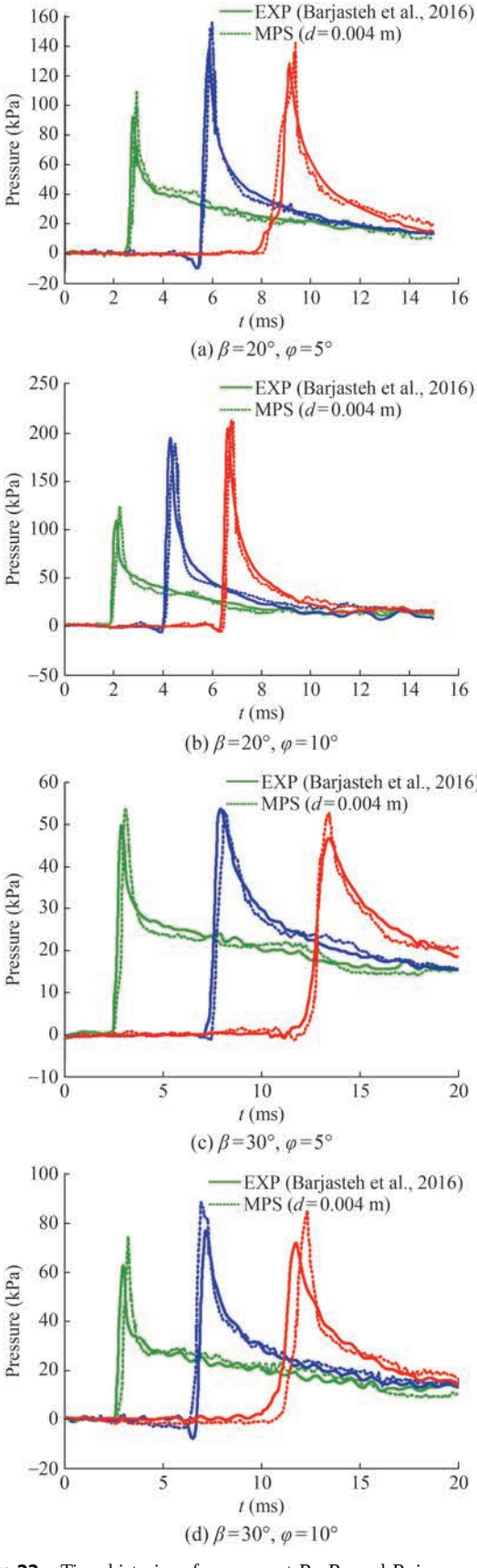

Figure 23 Time histories of pressure at P_1, P_2, and P_3 in asymmetric entry. (P_1: green; P_2: blue; P_3: red)

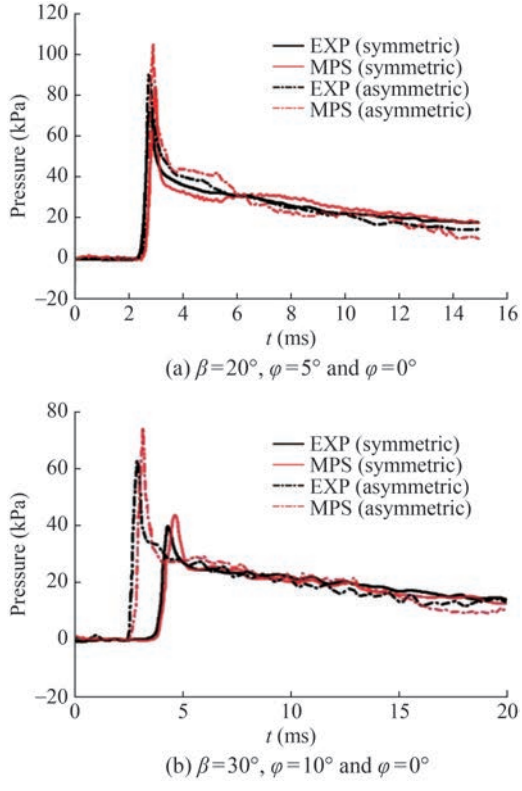

Figure 24 Time histories of pressure at P_1 in symmetric and asymmetric entry

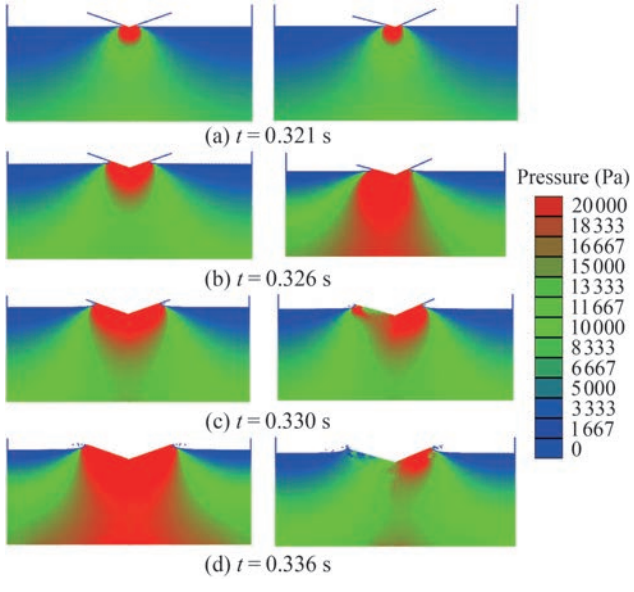

Figure 25 Pressure distributions at different times during symmetric and asymmetric entry (Left: β = 20°, φ = 0°; Right: β = 20°, φ = 5°)

pressure distributions around the wedge. These distributions can be attributed to not adopting a high-order Laplacian model. However, in Figure 26, large impact pressure occurs at a small dead-rise angle.

Overall, the above numerical results show that the present MPS method can provide a reliable solution for the 2D wedge water entry problem.

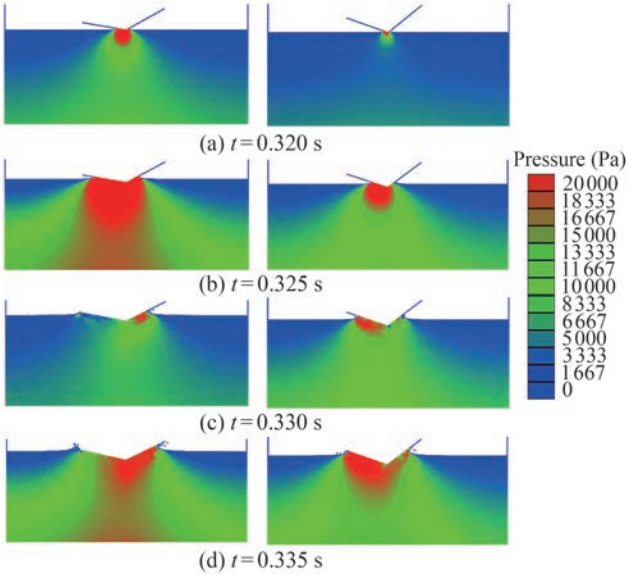

Figure 26 Pressure distributions at different times in different dead-rise angles (Left: β = 20°, φ = 10°; Right: β = 30°, φ = 10°)

4 Conclusions

This study examined the water entry of a 2D wedge. The main purpose was to verify the availability of investigations into water entry problems with the MPS method, and some techniques for enhancing the performance of the method were suggested, including the use of Laplacian compensation in the region close to the wall boundary and a collision model between fluid and wall particles. In addition, a symmetric domain technique for reducing computational cost and a fluid–solid-coupling algorithm using the MPS method were proposed.

The proposed techniques were validated through several numerical studies. First, hydrostatic pressure and dam break were simulated using the MPS method, and numerical results were compared with analytical solution and experimental results. Through these simulations, Laplacian compensation was found to greatly improve the performance of the method. Then, the water entry problems of the 2D wedge were investigated using the method. The simulations on water entry problems were compared with some experimental and previous numerical results. In the symmetric entry simulation, not only the accuracy of the MPS method was verified but also the effect of the symmetric domain technique was validated. The symmetric domain simulation resulted in nearly the same accuracy as the whole-domain simulation, whereas using half of the memory and consuming less time than the whole-domain simulation. In the asymmetric entry simulation, similar to the symmetric entry, the results of the MPS method agreed well with the experimental results, and a high impact pressure was obtained at a large inclination angle. Overall, our results suggest that the MPS method with the proposed techniques is suitable for simulating water entry problems.

However, the present study revealed some drawbacks, such as unstable pressure fluctuation and comparatively large errors. The experimental results were obtained from a 3D wedge, whereas our simulation was conducted on a 2D wedge. Moreover, owing to the limited computational capacity, relatively large particle spacings were selected in this study. Nevertheless, these limitations are expected to be overcome by introducing some advanced techniques, such as multi-GPU parallel computing and multiresolution processing. Another important limitation is that a higher-order Laplacian model was not adopted, which can improve the accuracy and stability of the MPS method. A solution to the above troubles will be carried out in future work.

Acknowledgement The authors would like to thank the anonymous reviewers for their constructive comments to help improve this paper greatly.

Competing interest The authors have no competing interests to declare that are relevant to the content of this article.

References

Amritkar A, Sturler ED, Świrydowicz K, Tafti D, Ahuja K (2015) Recycling Krylov subspaces for CFD applications and a new hybrid recycling solver. Journal of Computational Physics 303: 222-237. https://doi.org/10.1016/j.jcp.2015.09.040

Bao CM, Wu GX, Xu GD (2016) Simulation of water entry of a two-dimension finite wedge with flow detachment. Journal of Fluids and Structures 65: 44-59. https://doi.org/10.1016/j.jfluidstructs.2016.05.010

Bao CM, Wu GX, Xu G (2017) Simulation of freefall water entry of a finite wedge with flow detachment. Applied Ocean Research 65: 262-278. https://doi.org/10.1016/j.apor.2017.04.014

Barjasteh M, Zeraatgar H, Javaherian MJ (2016) An experimental study on water entry of asymmetric wedges. Applied Ocean Research 58: 292-304. https://doi.org/10.1016/j.apor.2016.04.013

Chen C, Zhang AM, Chen JQ, Shen YM (2021) SPH simulations of water entry problems using an improved boundary treatment. Ocean Engineering 238: 109679. https://doi.org/10.1016/j.oceaneng.2021.109679

Del Buono A, Bernardini G, Tassin A, Iafrati A (2021) Water entry and exit of 2D and axisymmetric bodies. Journal of Fluids and Structures 103: 103269. https://doi.org/10.1016/j.jfluidstructs.2021.103269

Farsi M, Ghadimi P (2015) Simulation of 2D symmetry and asymmetry wedge water entry by smoothed particle hydrodynamics method. Journal of the Brazilian Society of Mechanical Sciences and Engineering 37: 821-835. https://doi.org/10.1007/s40430-014-0212-5

Gotoh H, Khayyer A, Shimizu Y (2021) Entirely Lagrangian meshfree computational methods for hydroelastic fluid–structure interactions in ocean engineering—Reliability, adaptivity and generality. Applied Ocean Research 115: 102822. https://doi.org/10.1016/j.apor.2021.102822

Gu H, Qian L, Causon D, Mingham C, Lin P (2014) Numerical simulation of water impact of solid bodies with vertical and oblique entries. Ocean Engineering 75: 128-137. https://doi.org/10.1016/j.oceaneng.2013.11.021

Hestenes MR, Stiefel E (1952) Methods of conjugate gradients for solving linear systems. Journal of Research of the National Bureau of Standards 49(6): 409-436

Iafrati A, Battistin D (2003) Hydrodynamics of water entry in presence of flow separation from chines. Proceedings of the 8th International Conference on Numerical Ship Hydrodynamics 22-25

Judge C, Troesch A, Perlin M (2004) Initial water impact of a wedge at vertical and oblique angles. Journal of Engineering Mathematics 48: 279-303. https://doi.org/10.1023/B:engi.0000018187.33001.e1

Khayyer A, Shimizu Y, Gotoh H, Nagashima K (2021) A coupled incompressible SPH-Hamiltonian SPH solver for hydroelastic FSI corresponding to composite structures. Applied Mathematical Modelling 94: 242-271.https://doi.org/10.1016/j.apm.2021.01.011

Khayyer A, Gotoh H (2008) Development of CMPS method for accurate water-surface tracking in breaking waves. Coastal Engineering Journal 50(2): 179-207. https://doi.org/10.1142/S0578563408001788

Koshizuka S, Oka Y (1996) Moving-particle semi-implicit method for fragmentation of incompressible fluid. Nuclear Science and Engineering 123: 421-434. https://doi.org/10.13182/NSE96-A24205

Li ZP, Sun LQ, Yao XL, Wang DL, Li FC (2020) Experimental study on cavity dynamics in high froude number water entry for different nosed projectiles. Applied Ocean Research 102: 102305. https://doi.org/10.1016/j.apor.2020.102305

Lobovsky L, Botia-Vera E, Castellana F, Mas-Soler J, Souto-Iglesias A (2014) Experimental investigation of dynamic pressure loads during dam break. Journal of Fluids and Structures 48: 407-434. https://doi.org/10.1016/j.jfluidstructs.2014.03.009

Luo M, Khayyer A, Lin P (2021) Particle methods in ocean and coastal engineering. Applied Ocean Research 114: 102734. https://doi.org/10.1016/j.apor.2021.102734

Marrone S, Colagrossi A, Touze DL, Graziani G (2010) Fast free-surface detection and level-set function definition in SPH solvers. Journal of Computational Physics 229(10): 3652-3663. https://doi.org/10.1016/j.jcp.2010.01.019

Meng ZF, Ming FR, Wang PP, Zhang AM (2021) Numerical simulation of water entry problems considering air effect using a multiphase Riemann-SPH model. Advances in Aerodynamics 3: Article number: 13. https://doi.org/10.1186/s42774-021-00066-x

Oger G, Doring M, Alessanrini B, Ferrant P (2006) Two-dimensional SPH simulations of wedge water entries.Journal of Computational Physics 213(2): 803-822. https://doi.org/10.1016/j.jcp.2005.09.004

Piro DJ, Maki KJ (2013) Hydroelastic analysis of bodies that enter and exit water. Journal of Fluids and Structures 37: 134-150. https://doi.org/10.1016/j.jfluidstructs.2012.09.006

Riccardi G, Iafrati A (2004) Water impact of an asymmetric floating wedge. Journal of Engineering Mathematics 49: 19-39. https://doi.org/10.1023/B:ENGI.0000014885.89822.f5

Saad Y, Schultz MH (1986) GMRES: a generalized minimal residual algorithm for solving nonsymmetric linear systems. SIAM Journal on Scientific and Statistical Computing 7(3): 856-869. https://doi.org/10.1137/0907058

She WX, Zhou GL, Guo CY, Wu TC, Song KW (2021) Experimental investigation on the water entry of a bulbous bow based on TR-PIV. Ocean Engineering 229: 108977. https://doi.org/10.1016/j.oceaneng.2021.108977

Shibata K, Koshizuka S, Murotani K, Sakai M, Masaie I (2015a) Boundary conditions for simulating karman vortices using the MPS method. Journal of Advanced Simulation in Science and Engineering 2(2): 235-254. https://doi.org/10.15748/jasse.2.235

Shibata K, Masaie I, Kondo M, Murotani K, Koshizuka S (2015b) Improved pressure calculation for the moving particle semi-implicit method. Computational Particle Mechanics 2: 91-108. https://doi.org/10.1007/s40571-015-0039-6

Sun H, Faltinsen OM (2009) Water entry of a bow-flare ship section with roll angle. Journal of Marine Science Technology 14: 69-79. https://doi.org/10.1007/s00773-008-0026-1

Sun S, Wu GX, Xu G (2019) Free fall water entry of a wedge tank into calm water in three degrees of freedom. Applied Ocean Research 92: 101920. https://doi.org/10.1016/j.apor.2019.101920

Sun H, Faltinsen OM (2006) Water impact of horizontal circular cylinders and cylindrical shells. Applied Ocean Research 28(5): 299-311. https://doi.org/10.1016/j.apor.2007.02.002

Sun H (2007) A boundary element method applied to strongly nonlinear wave-body interaction problems. Trondheim: Norwegian University of Science and Technology

Sun Z, Korobkin A, Sui XP, Zhi Z (2021a) A semi-analytical model of hydroelastic slamming. Journal of Fluids and Structures 101: 103200. https://doi.org/10.1016/j.jfluidstructs.2020.103200

Sun YJ, Xi G, Sun ZG (2021b) A generic smoothed wall boundary in multi-resolution particle method for fluid-structure interaction problem. Computer Methods in Applied Mechanics and Engineering 378: 113726. https://doi.org/10.1016/j.cma.2021.113726

Sun P, Ming F, Zhang A (2015) Numerical simulation of interactions between free surface and rigid body using a robust SPH method. Ocean Engineering 98: 32-49. http://doi.org/10.1016/j.oceaneng.2015.01.019

Sun P, Zhang AM, Marrone S, Ming F (2018) An accurate and efficient SPH modeling of the water entry of circular cylinders. Applied Ocean Research 72: 60-75. https://doi.org/10.1016/j.apor.2018.01.004

Tveitnes T, Fairlie-Clarke AC, Varyani K (2008) An experimental investigation into the constant velocity water entry of wedge-shaped sections. Ocean Engineering 35(14-15): 1463-1478. https://doi.org/10.1016/j.oceaneng.2008.06.012

Von Karman TH (1929) The impact on seaplane floats during landing. Washington DC: NASA Report Number: NACA-TN-321

Wagner H (1932) The phenomena of impact and planning on water. Washington DC: NASA Technical Report 1366, NACA

Wang J, Lugni C, Faltinsen OM (2015) Experimental and numerical investigation of a freefall wedge vertically entering the water surface. Applied Ocean Research 51: 181-203. https://doi.org/10.1016/j.apor.2015.04.003

Wen P, Qiu W (2018) Improved prediction of 3-D water entry with a CIP method and parallel computing. Ocean Engineering 164: 426-442. https://doi.org/10.1016/j.oceaneng.2018.06.050

Wei ZY, Hu CH (2014) An experimental study on water entry of horizontal cylinders. Journal of Marine Science Technology 19: 338-350. https://doi.org/10.1007/s00773-013-0252-z

Wei ZY, Hu CH (2015) Experimental study on water entry of circular cylinders with inclined angles. Journal of Marine Science Technology 20: 722-738. https://doi.org/10.1007/s00773-015-0326-1

Wu G (2012) Numerical simulation for water entry of a wedge at varying speed by a high order boundary element method. Journal of Marine Science and Application 11: 143-149. https://doi.org/10.1007/s11804-012-1116-3

Xu GD, Duan WY, Wu GY (2008) Numerical simulation of oblique water entry of an asymmetrical wedge. Ocean Engineering 35(16): 1597-1603. https://doi.org/10.1016/j.oceaneng.2008.08.002

Xu L, Troesch AW, Peterson R (1999) Asymmetric hydrodynamic impact and dynamic response of vessels. J. Offshore Mech. Arctic Eng. 121: 83-89. https://doi.org/10.1115/1.2830082

Yettou EM, Desrochers A, Champoux Y (2006) Experimental study on the water impact of a symmetrical wedge. Fluid Dynamics Research 38(1): 47-66. https://doi.org/10.1016/j.fluiddyn.2005.09.003

Yu P, Li H, Ong MC (2019) Hydroelastic analysis on water entry of a constant-velocity wedge with stiffened panels. Marine Structures 63: 215-238. https://doi.org/10.1016/j.marstruc.2018.09.007

Zekri HJ, Korobkin AA, Cooker MJ (2021) Gravity effect on water entry during an early stage. Journal of Fluid Mechanics 916: A10. https://doi.org/10.1017/jfm.2021.190

Zha RS, Peng H, Qiu W (2021) An improved higher-order moving particle semi-implicit method for simulations of two-dimensional hydroelastic slamming. Physics of Fluids 33: 037104. https://doi.org/10.1063/5.0033491

Zhao ZX, Bilotta G, Yuan QE, Gong ZX, Liu X (2023) Multi-GPU multi-resolution SPH framework towards massive hydrodynamics simulations and its applications in high-speed water entry. Journal of Computational Physics 490: 112339. https://doi.org/10.1016/j.jcp.2023.112339

Zhang HS, Zhang ZL, He F, Liu MB (2022a) Numerical investigation on the water entry of a 3D circular cylinder based on a GPU-accelerated SPH method. European Journal of Mechanics/B Fluids 94: 1-16. https://doi.org/10.1016/j.euromechflu.2022.01.007

Zhang K, Sun YJ, Sun ZG, Wang F, Chen X, Xi G (2022b) An efficient MPS refined technique with adaptive variable-size particles. Engineering Analysis with Boundary Elements 143: 663-676. https://doi.org/10.1016/j.enganabound.2022.07.013

Zhao R, Faltinsen O, Aarsnes J (1996) Water entry of arbitrary two-dimensional sections with and without flow separation. Twenty-First Symposium on Naval Hydrodynamics 408-423

Zhang G, Feng S, Zhang Z, Chen Y, Sun Z, Zong Z (2021) Investigation of hydroelasticity in water entry of flexible wedges with flow detachment. Ocean Engineering 222: 108580. https://doi.org/10.1016/j.oceaneng.2021.108580